Silicon
DOI 10.1007/s12633-016-9513-x

ORIGINAL PAPER

# Structural, Electrical and Photoresponse Properties of Si-based Diode with Organic Interfacial Layer Containing Novel Cyclotriphosphazene Compound

**A. Tataroğlu[1] · Furkan Özen[2] · Kenan Koran[2] · A. Dere[3] · Ahmet Orhan Görgülü[2] · Norah Al-Senany[4] · Ahmed Al-Ghamdi[4] · W. A. Farooq[5] · F. Yakuphanoglu[3]**

Received: 9 October 2016 / Accepted: 19 October 2016


**Abstract** The electrical and photoresponse properties of an Al/p-Si/organic layer/Al diode were investigated. The organic layer containing novel 2,2-bis[spiro(7,8-dioxy-4-methylcoumarin)]-4,4,6,6-bis[spiro(2',2"-dioxy-1',1"-biphenylyl)]cyclotriphosphazene compound was coated by the drop casting method on p-Si having ohmic contact. The structural characterization of the novel cyclotriphosphazene compound was confirmed by using $^{1}H$, $^{13}C$ and $^{31}P$-NMR, elemental analysis and FTIR spectroscopic techniques. The diode exhibits a photoconducting and photodiode behavior under solar light illumination. The electrical parameters such as ideality factor, barrier height and series resistance of the diode were determined from I-V characteristics. It is seen that the photocurrent of the diode under illumination is higher than the dark current. Also, the frequency dependence of capacitance (C) and conductance (G) was explained on the basis of interface states. It is evaluated that the hybrid photodiode can be used as a photosensor in organic photodetector applications.

**Keywords** Organic photovoltaic diode · Cyclotriphosphazene · Coumarin-phosphazene

✉ F. Yakuphanoglu
fyhan@hotmail.com

[1] Department of Physics, Faculty of Science, Gazi University, Ankara, Turkey

[2] Department of Chemistry, Faculty of Science, Fırat University, Elazıg, Turkey

[3] Department of Physics, Faculty of Science, Fırat University, Elazıg, Turkey

[4] Department of Physics, Faculty of Sciences, King Abdulaziz University, Jeddah, Saudi Arabia

[5] Department of Astronomy and Physics, College of Science, King Saud University, Riyadh, Saudi Arabia

## 1 Introduction

Cyclotriphosphazenes have a characteristic ring structure comprising of phosphorus (P) and nitrogen (N) atoms [1]. Cyclotriphosphazenes are one of the major classes of phosphazene compounds. Phosphazenes, which consist of repeating units of –P=N– in their structure, are chemical compounds having linear or cyclic structure connected to the two organic or inorganic side groups (R) of each phosphorus atom. Due to the reactivity of the -Cl atom in their structure, the type of organic or inorganic group bonded as side groups to the phosphazene compounds changes physical, biological and chemical properties of these compounds [2–4]. Phosphazene compounds have been used in many applications such as liquid crystals [5], polymer solid electrolytes [6], cathode material for rechargeable lithium batteries [7], flame retardants [8, 9], organic light emitting diodes and fluorescence sensors [10–13]. These compounds exhibit numerous properties such as high thermal and chemical stability [14, 15], biocompatibility [16, 17], gas permeability [18], and high conductivity [19].

Coumarin derivatives are an important group of compounds of synthetic and natural organic chemistry. The compounds with a carbonyl group in the $\alpha$-position of the benzopyrane ring are called coumarin (2H-1-benzopyrane-2-one). Coumarin analogs possess different physical and

Published online: 23 March 2017

biological properties such as antioxidants, fluorescent chemosensors, lasers, antifungal, anticoagulant, stabilizers and anticancer agent [20–24].

Although there are many reports on the synthesis of substituted cyclotriphosphazene derivatives [25–29], there is no study about synthesis of the cyclotriphosphazene derivatives bearing dihydroxycoumarin groups.

Therefore, firstly, the novel 2,2-bis[spiro(7,8-dioxy-4-methylcoumarin)]-4,4,6,6-bis[spiro(2',2"-dioxy-1',1"-biphenylyl)]cyclotriphosphazene 2 was prepared by the reaction of 2,2-dichloro-4,4,6,6-bis[spiro(2',2"-dioxy-1',1" -biphenylyl]cyclotriphosphazene 1 with 7,8- dihydroxy-4-methylcoumarin in the $Cs_2CO_3$/xylene system for the first time. In other words, 7,8-dihydroxy-4-methylcoumarin was reacted with compound 1 in order to get substituted cyclotriphosphazene 2. Dioxycoumarin substituted cyclophosphazene 2 was designed, synthesized and characterized by $^{1}H$, $^{13}C$, $^{31}P$-NMR elemental analysis and FTIR spectroscopic techniques. The optoelectronic properties of the fabricated Al/p-Si/organic layer/Al diode were investigated by electrical and impedance spectroscopy techniques.

## 2 Experimental Details

### 2.1 Materials and Methods

Hexachlorocyclotriphosphazene, $N_3P_3Cl_6$(TCI), was purified by the crystallization from n-hexane. 7,8-dihydroxy-4-methylcoumarin and 2,2'-dihydroxybiphenyl were obtained from Sigma Aldrich and Merck, respectively. The solvents were obtained from Merck.

$^{1}H$, $^{13}C$ and $^{31}P$-NMR spectra were recorded in chloroform-d solutions on a Bruker DPX 400 MHz spectrometer using TMS (an internal reference for $^{1}H$-NMR) and 85% $H_3PO_4$ (an external reference for $^{31}P$-NMR). Microanalysis and FTIR spectrum were obtained using a Leco 932 CHNS-O apparatus and PerkinElmer FTIR spectrometer, respectively.

### 2.2 Synthesis

Biphenyl substituted cyclotriphosphazene 1 was obtained and purified as defined by Carriedo et al. [30].

#### *2.2.1 Preparation of 2,2-bis[spiro(7,8-dioxy-4-methylcoumarin)]-4,4,6,6-bis[spiro(2',2"-dioxy-1',1"-biphenylyl)]cyclotriphosphazene 2*

Compound 1 (1.0 g, 1.75 mmol) and $Cs_2CO_3$ (0.67 g, 2.08 mmol) were dissolved in 30 mL of dry xylene (mixture of isomers) in a 100 mL two-necked reaction flask. 7,8-Dihydroxy-4-methylcoumarin (0.36 g, 0.52 mmol) in 20 mL of dry xylene was slowly added to the stirred solution at 0 °C. The reaction mixture was stirred and refluxed in xylene for 24 h. After cooling the reaction mixture, the mixture was filtered to remove the formed cesium chloride. Xylene was removed by a rotary evaporator. The resulting light yellow solid was redissolved in 10 mL of xylene and then poured into n-hexane. The precipitate was filtered and dried in a vacuum. The product was purified by column chromatography using chloroform as the mobile phase. Chloroform was removed on a rotary evaporator. The pure white product (2) formed 0.23 g (60%). Anal. Calc. for $C_{34}H_{22}N_3O_8P_3$(MW = 693.47 g/mol): C, 58.89; H, 3.20; N, 6.06. Found: C, 58.71; H, 3.35; N, 6.18%. FTIR (KBr, $cm^{-1}$): 3027 and 3065 $\nu_{C-H(Aromatic)}$, 2917 and 2956 $\nu_{C-H(Aliphatic)}$, 1751 $\nu_{C=O}$, 1499, 1588 and 1634 $\nu_{C=C}$, 1175 and 1193 $\nu_{P=N}$, 974 $\nu_{P-O-C}$. $^{31}P$ NMR ($CDCl_3$) $\delta$/ppm: 24.63 (2P, d, $P_a(O_2C_{12}H_8)$), 36.66 (1P, t, $P_b(O_4C_{10}H_6)$). $^{1}H$ NMR ($CDCl_3$)$\delta$/ppm: 2.42 (3H, s, $H^{16}$), 6.34 (1H, s, $H^{14}$), 7.01-7.58 (18H, m, $H^3$, $H^4$, $H^5$, $H^{11}$ and $H^{12}$). $^{13}C$ NMR ($CDCl_3$)$\delta$/ppm: 147.79 $C^1$, 128.49 $C^2$, 126.48 $C^3$, 129.84 $C^4$, 130.11 $C^5$, 122.06 $C^6$, 147.82 $C^7$, 152.52 $C^8$, 153.94 $C^9$, 128.67 $C^{10}$, 113.68 $C^{11}$, 118.93 $C^{12}$, 116.65 $C^{13}$, 108.68 $C^{14}$, 159.05 $C^{15}$ and 19.05 $C^{16}$.

### 2.3 Fabrication of Al/p-Si/organic Layer/Al Diode

Before forming the organic layer on the p-Si substrate, the native oxide layer of p-Si was etched by HF. Subsequently, the Si substrate was ultrasonically cleaned in a bath of deionized water for 10-15 min, followed by chemical baths of methanol and acetone. Afterwards, a solution of 2,2-bis[spiro(7,8-dioxy-4-methylcoumarin)]-4,4,6,6-bis[spiro(2',2"-dioxy-1',1"-biphenylyl)]cyclotriphosphazene compound (2) was prepared and it was coated by the drop coating method on p-Si having aluminum (Al) ohmic contact. Then, it was dried at 50 °C for 10 min. Ohmic contact was prepared by evaporating aluminum metal on the silicon wafer at $5\times10^{-5}$ Torr and annealing at 570 °C for 5 min in a nitrogen atmosphere. Top contact was prepared by Al metal on the organic layer. A diode contact area of $7.85\times10^{-3}$ was formed by evaporating Al metal on the organic layer. Structural characterization of compound 2 was performed using $^{1}H$, $^{13}C$ and $^{31}P$-NMR, elemental analysis and FTIR spectroscopic techniques. Electrical measurements of the diode were carried out using a FYtronix Electronic Device characterization system (Fig. 1a) at room temperature. Photoelectrical measurements of the diode were done in dark and illumination conditions The intensity of solar light is controlled using a FYtronix Electronic Device characterization system.

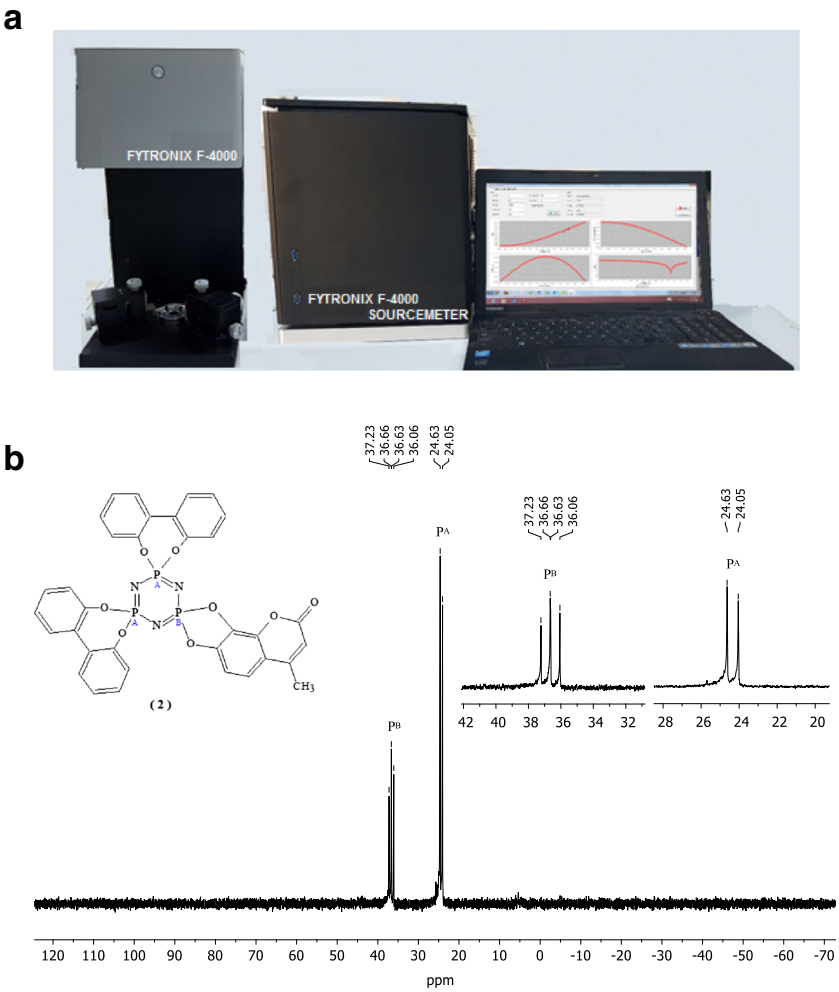


**Fig. 1** **a** FYTRONIX Electronic Device characterization system. **b** $^{31}$P-NMR spectrum of compound **2** (chloroform-d)

## 3 Results and Discussion

### 3.1 Synthesis

2,2-Dichloro-4,4,6,6-bis[spiro(2',2"-dioxy-1",1"-biphenyl] cyclotriphosphazene 1 was prepared from the interaction of $N_3P_3Cl_6$(HCCP) with 2,2'-biphenol under an argon atmosphere [30]. The reactions of compound 1 with 1.1 equiv. of 7,8-dihydroxycoumarin in the presence of $Cs_2CO_3$ in dry xylene (mixture of isomers) gave the substituted cyclotriphosphazene 2. The structure of dioxycoumarin-cyclotriphosphazene 2 was confirmed by $^1$H, $^{13}$C and $^{31}$P-NMR, elemental analysis and FTIR spectroscopy techniques. General presentation of cyclotriphosphazene compounds 1 and 2 is shown in Scheme 1.

The OH stretching vibrations were not observed in the FTIR spectra of compound 2. The absence of the OH peaks in the FTIR spectra of 2 indicates that all hydrogen atoms of the OH groups have been replaced. The aromatic (-CH) stretching frequencies were at 3027 and 3065 cm$^{-1}$. The carbonyl group in the structure of coumarin was observed at 1751 cm$^{-1}$. The -P=N stretching frequencies, which are between 1175 and 1193 cm$^{-1}$, are characteristic of cyclotriphosphazene derivatives. The P-O-C stretching vibration was observed at 974 cm$^{-1}$.

The $^{31}$P NMR spectrum for compound 2 is given in Fig. 1b ($AB_2$ system). There are two peaks in the $^{31}$P NMR spectrum of the coumarin substituted cyclotriphosphazene compound. The $^{31}$P NMR spectrum of 2 gives two sets of peaks around $\delta$ = 24.63 and 36.66 ppm in a doublet-triplet.

The $^1$H and $^{13}$C-NMR data also confirm the structure of compound 2 (Scheme 1). The characteristic peaks in the $^1$H and $^{13}$C-NMR spectra of 2 are given in the Experimental section. In the $^1$H-NMR spectra of 2, the absence of the OH protons indicates the coumarin substituted cyclotriphosphazene compound. The methyl protons for the compound 2 were observed at 2.42 ppm. The aromatic protons for 2 appear between 7.01 and 7.58 ppm. The $^{13}$C-NMR spectrum of 2 is depicted in Fig. 2. The carbonyl carbon peak (C=O, $C^{15}$) for 2 was at 159.05 ppm. The methyl carbon for 2 was observed at 19.05 ppm.

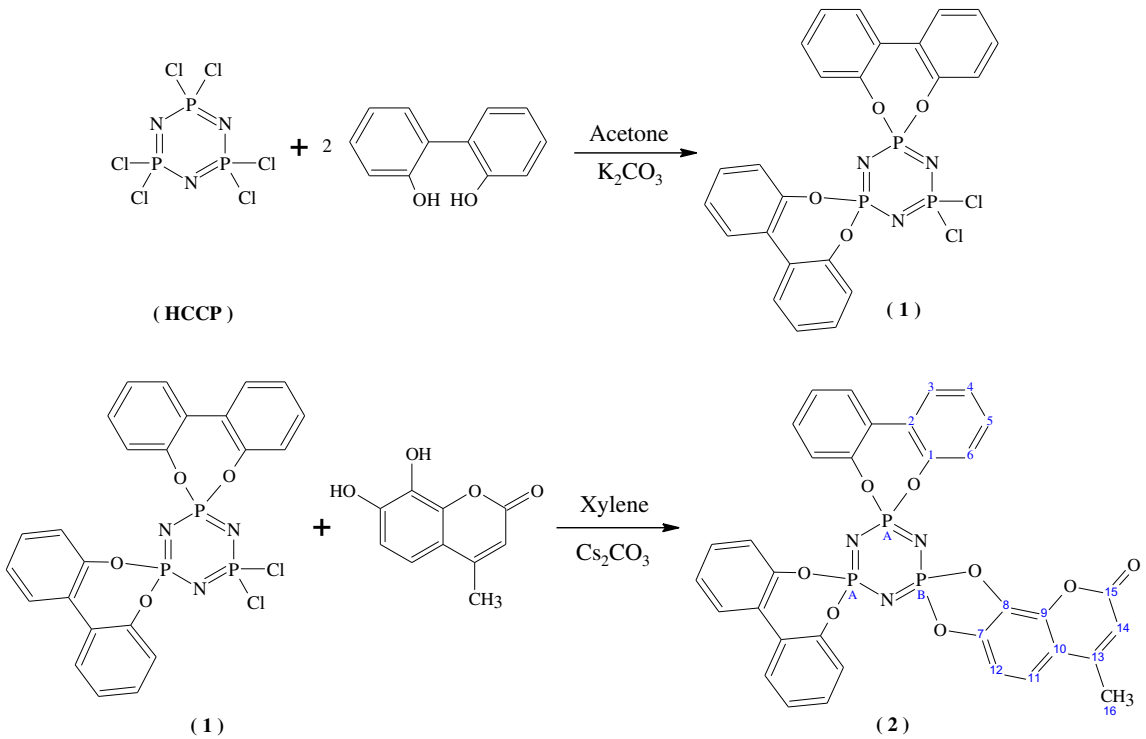


**Scheme 1** General presentation of the reactions

### 3.2 Photocurrent-voltage (I-V) Characteristics of the Diode

The electrical behavior of a typical Schottky diode can be analyzed by conventional thermionic emission (TE) theory. In Schottky barrier diodes, the current (I) is due to thermionic emission of electrons over the barrier. In this theory, the current is expressed by the following relation [31–33].

$$I = I_0 \left[ \exp\left( \frac{q(V - IR_s}{nkT} \right) - 1 \right] \quad (1)$$

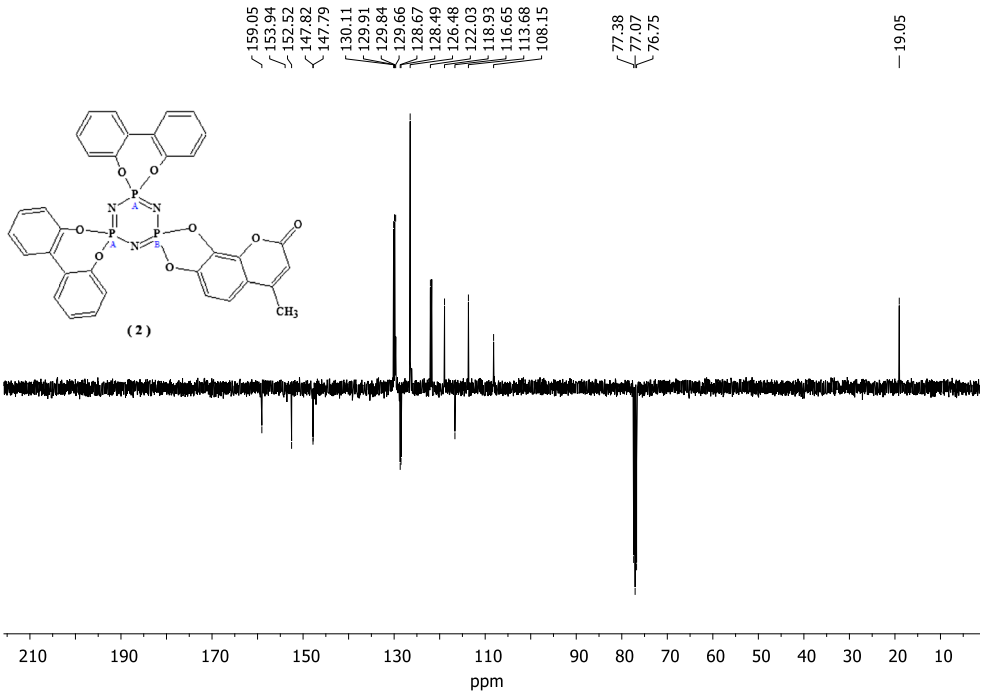


**Fig. 2** $^{13}$C-NMR spectrum of compound **2** (chloroform-d)

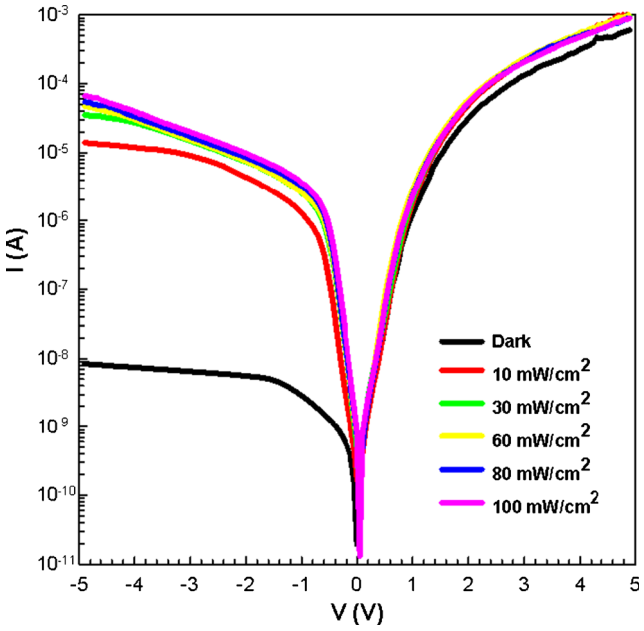


**Fig. 3** I-V characteristics of the diode under dark and illumination conditions

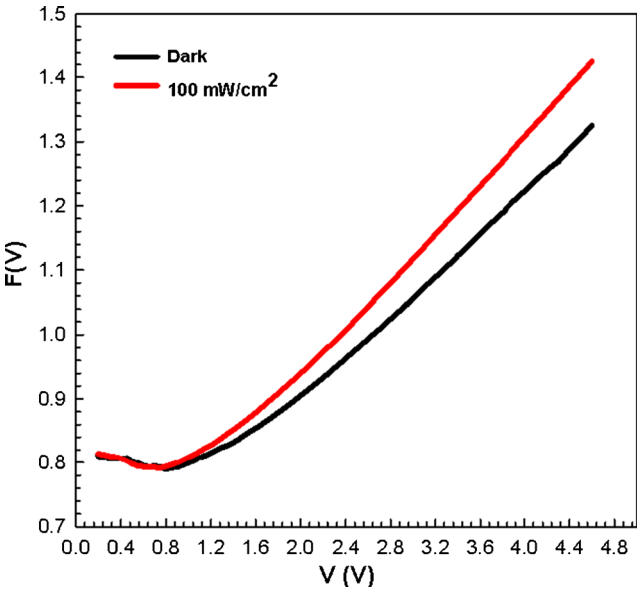


**Fig. 4** Plots of F(V) vs. V of the diode for dark and 100 mW/cm$^2$

where k is the Boltzman's constant, T is the absolute temperature, $R_s$ is the series resistance n is the ideality factor, and for forward values of V in excess of 3kT/q, a plot of ln I against V gives a straight line. $I_0$ is the reverse saturation current given by the following equation

$$I_o = A\ A^*\ T^2\ \exp\left(-\frac{q\Phi_b}{kT}\right) \tag{2}$$

where $\Phi_b$ is the barrier height, A is the diode contact area, and A* is the Richardson constant (32 A/cm$^2$.K$^2$ for p-type Si). The barrier height is obtained by Eq. (2). The ideality factor is expressed by the following equation

$$n = \frac{q}{kT}\left(\frac{dV}{d(\ln I)}\right) \tag{3}$$

Dark and photoelectrical (I-V) characteristics of the diode are given in Fig. 3. As seen in Fig. 3, the fabricated diode shows a rectifying behavior in the dark, and the value of the current under illumination is substantially higher than its value in the dark. Also, reverse current under illumination called as a photocurrent while the forward current is almost unchanged with illumination. This confirms the photoconductive behavior of the diode. Upon illumination of the diode, a photocurrent is created by the photo-generated charge carriers at the interface on the diode [34–39]. The value of ideality factor and barrier height determined from the forward bias I-V characteristics for dark and 100 mW/cm$^2$ is given in Table 1. The obtained ideality factor value is higher than unity due to series resistance, inhomogeneities of barrier height and interface states [40–45]. In addition, the series resistance affects the linear region of forward bias I-V curves and in turn, the linear region deviates from linearity.

The electrical parameters such as barrier height and series resistance of the diode were also extracted by using another method proposed by Norde [46–48]. In this method, the Norde function can be defined as

$$F(V) = \frac{V}{\gamma} - \frac{kT}{q}\ln\left(\frac{I}{AA^*T^2}\right) \tag{4}$$

where $\gamma$ is an integer which is greater than the ideality factor. The barrier height for the diode is obtained by the following equation

$$\Phi_{B0} = F(V_{\min}) + \frac{V_{\min}}{\gamma} - \frac{kT}{q} \tag{5}$$

**Table 1** Electrical parameters of the diode derived from I-V characteristics and the Norde method

| P(mW/cm$^2$) | n (I-V) | $\Phi_b$(eV) (I-V) | $\Phi_b$(eV) (Norde) | $R_s$(kΩ) (Norde) |
|---|---|---|---|---|
| Dark | 4.29 | 0.82 | 0.90 | 59.22 |
| 100 | 3.95 | 0.83 | 0.91 | 33.59 |

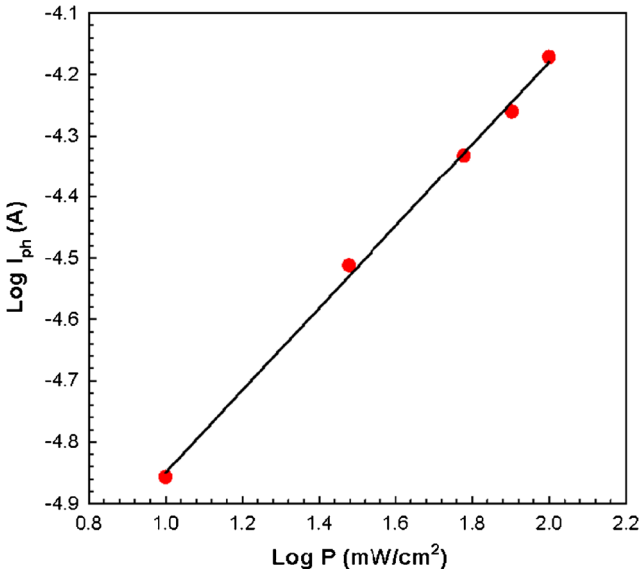


**Fig. 5** Plot of log($I_{ph}$) vs. log(P) of the diode (at −5 V)

where $F(V_{min})$ is the minimum value of F(V). In the Norde method, the series resistance ($R_s$) is expressed by the following relation

$$R_s = \frac{kT(\gamma - n)}{qI_{min}} \tag{6}$$

where $I_{min}$ is the current in the diode corresponding to voltage $V_{min}$.

The plots of the Norde function F(V) versus V of the diode for dark and 100 mW/cm$^2$ are given in Fig. 4. A minimum point in F(V)-V plots was observed, as seen in Fig. 4. The calculated values of $\Phi_b$ and $R_s$ are given in Table 1. The $\Phi_b$ values obtained from both the Norde function and I-V characteristics are close to each other. The $R_s$ value is quite high due to the electrical conductivity of the organic layer.

The photoconducting behavior of the diode can be analyzed by using the following relation [49–52],

$$I_{ph} = BP^m \tag{7}$$

where B is a constant, P is the illumination intensity, $I_{ph}$ is the photocurrent and m is an exponent determining the photoconduction mechanism. The variation of photocurrent with illumination of the diode is given in Fig. 5. The value of m was determined from the slope of the log($I_{ph}$) vs. log(P) plot, and it was calculated to be about 0.67. The obtained m value indicates that the photoconducting mechanism is controlled by the presence of the trap centers.

### 3.3 Transient Photocurrent, Photocapacitance and Photoconductance Measurements

The photoconduction mechanism of the diode can be analyzed by the transient photocurrent-time measurements. Figure 6 shows current-time measurements of the diode. As seen in Fig. 6, the photocurrent increases quickly up to a certain level in the switching on state. The increase is due to the increase in the number of free charge carriers. In the switching off state, the photocurrent decreases quickly and comes back to its original level. Trapped charge carriers in the deep levels cause a decrease in current [52–56].

In addition, the dynamic transient photocapacitance and photoconductance characteristics of the diode were measured and are given in Fig. 7 (a) and (b), respectively. As seen in these figures, the photocapacitance value increases while the photoconductance value decreases with increasing illumination intensity. In the switching on and off states,

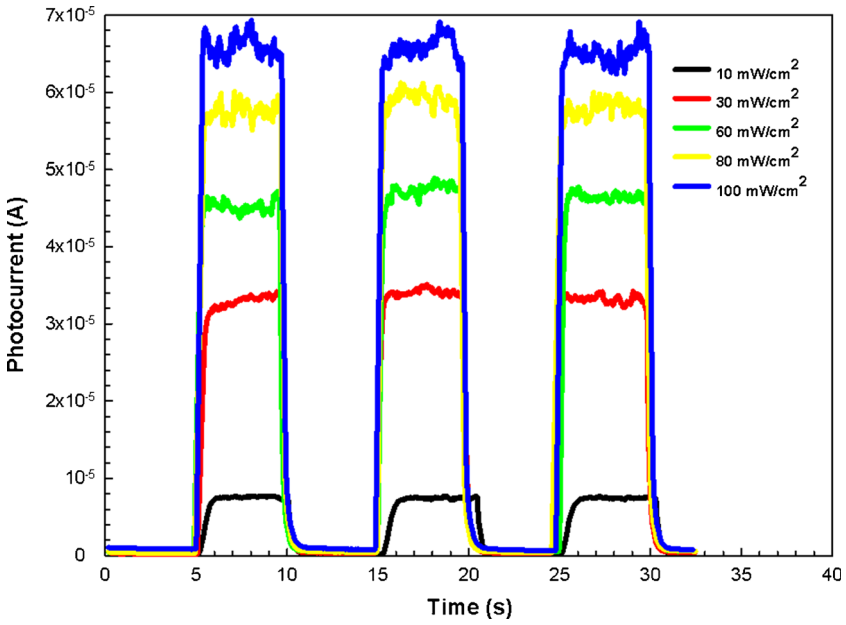


**Fig. 6** Transient photocurrent measurements of the diode at various illumination intensities and -5 V

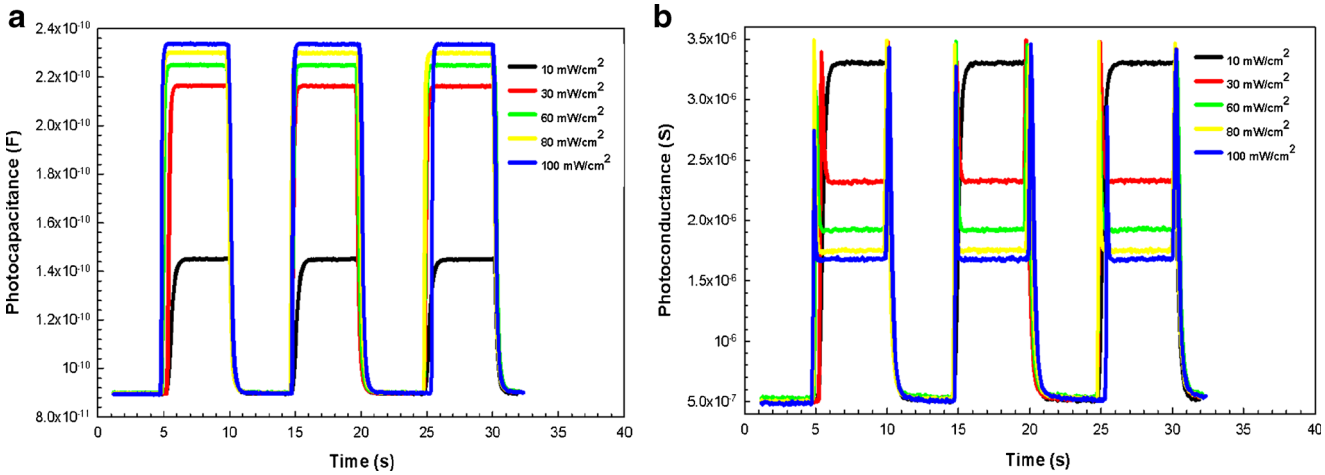


**Fig. 7** Transient (**a**) photocapacitance (**b**) photoconductance measurements at various illumination intensities and 10 kHz

a sudden change in the photocapacitance and photoconductance is taking place, i.e, the capacitance is increased with illumination. This confirms the photocapacitor behavior of the diode.

### 3.4 Capacitance/conductance-voltage (C/G-V) Measurements

The C-V) and G-V plots of the diode at various frequencies are given in Fig. 8 (a) and (b), respectively. It is seen in Fig. 8 (a) that the capacitance is decreased with increasing frequencies in the reverse bias region, whereas it did not change with frequency. A peak was observed in the C-V curves of the diode. This resulted from the interface states in the negative voltage region. The increasing frequency causes a decrease in peak intensity. This decrease suggests that the interface charges in the interface of the diode follow the frequency of the applied electric field. The conductance value increases with frequency, as seen in Fig. 8 (b). The change is explained by the presence of interface states [56–59]. The lowest peak intensity in the C-V plots suggests that the interface states at the higher frequencies are non-dispersive.

The series resistance profile is important to understand the charge transport mechanism. To analyze this effect, we measured the series resistance ($R_s$) of the diode and it was analyzed with the conductance method. In the conductance method, $R_s$ is expressed as follows [60]

$$R_s = \frac{G_{ma}}{G_{ma}^2 + (\omega C_{ma})^2} \tag{8}$$

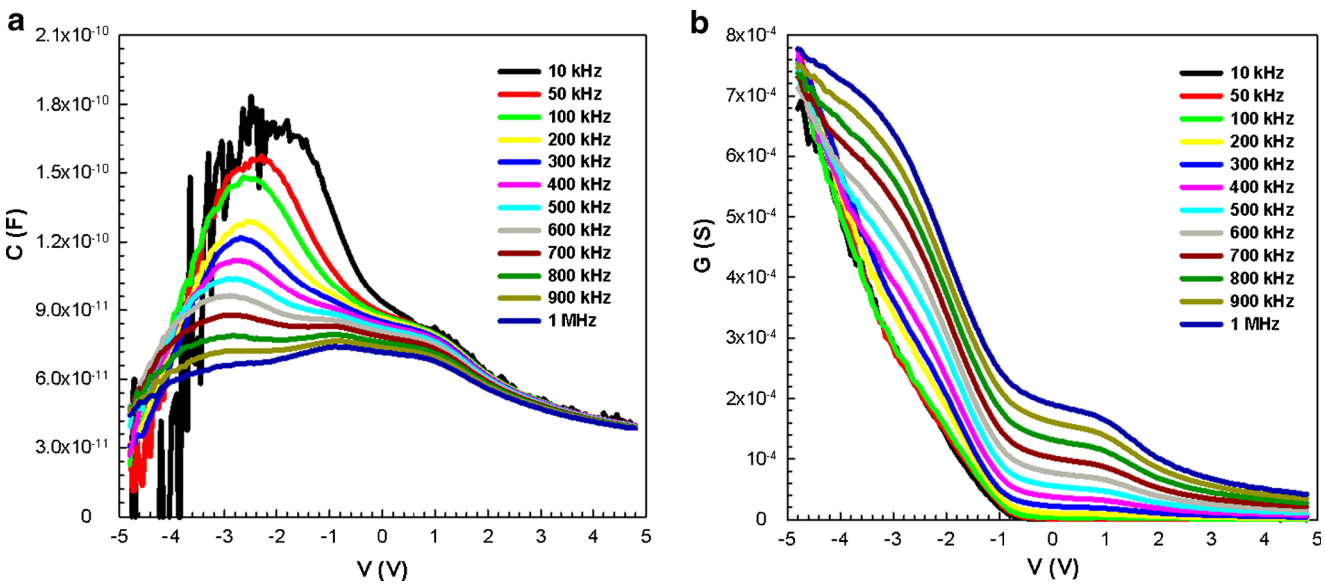


**Fig. 8** **a** CV (**b**) GV plots at various frequencies

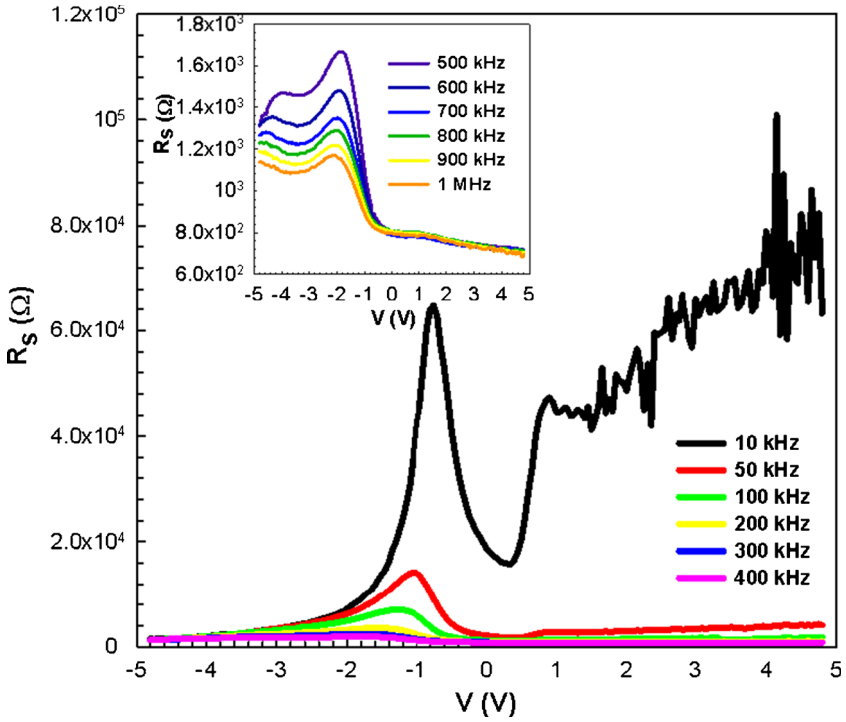


**Fig. 9** $R_s$V plots of the diode at various frequencies

where $C_{ma}$ is the measured capacitance, and $G_{ma}$ is the measured conductance. The series profile under various frequencies is shown in Fig. 9. The series resistance plots exhibit a peak due to the presence of the interface states. The peak intensity is decreased with increasing frequency. The change in $R_s$ is indicative of interface charges following the frequency of the applied electric field. The peak intensity is related to the number of interface states under various frequencies [61–64].

## 4 Conclusions

The photoelectrical properties of the fabricated Al/p-Si/organic layer/Al diode were analyzed in detail. I-V characteristics under illumination indicate that the diode exhibited a photodiode behavior. The photodiode behavior of the diode is explained by the transient photocurrent, photocapacitance and photoconductance measurements. The photodiode exhibited a high photoresponsivity. The photoelectrical results show that the fabricated photodiode can be used as a photosensor in organic photodetector applications.

**Acknowledgments** The authors are grateful to the Research Fund of the TUBITAK for their support (for the synthesis of compounds) with the project No-110T652. The authors extend their appreciation to the International Scientific Partnership Program ISPP at King Saud University for funding this research work through ISPP# 0046.

## References

1. Liu H, Wang X, Wu D (2014) Polym Degrad Stab 103:96–112
2. Allcock HR (1972) Phosphorus-nitrogen compounds. Cyclic, linear, and high polymeric systems. Academic Press, New York
3. Trinquier G (1986) J Am Chem Soc 108:568–577
4. Koran K, Özen F, Biryan F, Görgülü AO (2016) J Molec Struct 1105:135–141
5. Moriya K, Suzuki T, Yano S, Miyajima S (2001) J Phys Chem B 105:7920–7927
6. Zhou S, Fang S (2007) Eur Polym J 43:3695–3700
7. Xu GX, Lu Q, Yu BT, Wen L (2006) Solid State Ionics 177:305–309
8. Reed CS, Taylor JP, Guigley KS, Coleman MM, Allcock HR (2000) Polym Eng Sci 40:465–472
9. Liu R, Wang X (2009) Polym Degrad Stab 94:617–624
10. Franc G, Mazeres S, Turrin C-O, Vendier L, Duhayon C, Caminade AM, Majoral JP (2007) J Org Chem 72:8707–8715
11. Xu J, Toh CL, Ke KL, Li JJ, Cho CM, Lu X, Tan EW, He C (2008) Macromolecules 41:9624–9636
12. Şenkuytu E, Eçik ET, Durmuş M, Çiftçi GY (2009) Polyhedron 101:223–229
13. Özcan E, Tümay SO, Alidağı HA, Çoşut B, Yeşilot S (2016) Dyes and Pigments 132:230–236
14. Chen YM, Liao YL, Lin JJ (2010) J Colloid Interface Sci 343:209–216
15. Koran K, Özen F, Biryan F, Demirelli K, Görgülü AO (2016) Inorg Chim Acta 450:162–169
16. Siwy M, Seük D, Kaczmarczyk B, Jaroszewicz I, Nasulewicz A, Pelczynska M, Nevozhay D, Opolski A (2006) J Med Chem 49:806–810
17. Brandt K, Kruszynski R, Bartzak TJ, Czomperlik IP (2001) Inorg Chim Acta 322:138–144
18. Drioli E, Zhang SM, Basili A, Golemme G, Gaeta SN, Zhang HC (1991) Gas Sep Purif 5:252–258

19. Alidağı HA, Gırgıç ÖM, Zorlu Y, Hacıvelioğlu F, Çelik SÜ, Bozkurt A, Kılıç S, Yeşilot S (2013) Polymer 54:2250–2256
20. Danko M, Szabo E, Hrdlovic P (2011) Dyes Pigm 90:129–138
21. Zhou Z, Li N, Tong A (2011) Anal Chim Acta 702:81–86
22. Stanchev S, Hadjimitova V, Traykov T, Boyanov T, Manolova I (2009) Eur J Med Chem 44:3077–3082
23. Zaki RM, Elossaily YA, El-Dean AMK, Russian J (2012) Bioorganic Chem 38:639–646
24. Weigt S, Hübler N, Strecker R, Braunbeck T, Broschard TH (2012) Reprod Toxicol 33:133–141
25. Koran K, Ozen F, Torğut G, Pıhtılı G, Cil E, Arslan M, Görgülü AO (2014) Polyhedron 79:213–220
26. Çoşut B (2014) Dyes Pigm 100:11–16
27. Harrup MK, Rollins HW, Jamison DK, Dufek EJ, Gering KL, Luther TA (2015) J Power Sources 278:794–801
28. Fei S-T, Lee S-HA, Pursel SM, Basham J, Hess A, Grimes CA, Horn MW, Mallouk TE, Allcock HR (2011) J Power Sources 196:5223–5230
29. Bolink HJ, Barea E, Costa RD, Coronado E, Sudhakar S, Zhen C, Sellinger A (2008) Org Electron 9:155–163
30. Carriedo GA, Catuxo LF, Alonso FJG, Elipe PG, González PA (1996) Macromolecules 29:5320–5325
31. Dere A (2015) Journal of Materials and Electronic Devices 1:7–10
32. Altındal Ş (2015) Journal of Materials and Electronic Devices 1:42–47
33. Ilhan M (2015) Journal of Materials and Electronic Devices 1:15–20
34. Aksu Canbay C, Tataroglu A, Dere A, Al-Ghamdi A, Yakuphanoglu F (2016) J Alloys Compd 688:762–768
35. Singh J (2003) Electronic and Optoelectronic Properties of Semiconductor Structures. Cambridge University Press, New York
36. Tataroglu A, Dayan O, Ozdemir N, Serbetci Z, Al-Ghamdi AA, Dere A, El-Tantawy F, Yakuphanoglu F (2016) Dyes Pigm 132:64–71
37. Ocaya RO, Al-Ghamdi A, Mensah-Darkwa K, Gupta RK, Farooq W, Yakuphanoglu F (2016) Synth Met 213:65–72
38. Tan SO, Uslu Tecimer H, Cicek O, Tecimer H, Orak I, Altındal S (2016) J Mater Sci Mater Electron 27:8340–8347
39. Soliman HS, Farag AAM, Saadeldin MM, Sawaby K (2015) Acta Phys Pol A 127:1688–1693
40. Tung RT (2001) Phys Rev B 64:205310
41. Thapaswini PP, Padma R, Balaram N, Bindu B, Reddy VR (2016) Superlatt Microstruc 93:82–91
42. Mamor M, Bouziane K, Tirbiyine A, Alhamrashdi H (2014) Superlat Microstruct 72:344–351
43. Kaushal P, Chand S, Osvald J (2013) Int J Electron 100:686–698
44. Tataroglu A, Altındal S (2009) J Alloys Compd 479:893–897
45. Aydın H, Tataroglu A, Al-Ghamdi AA, Yakuphanoglu F, El-Tantawy F, Farooq WA (2015) J Alloys Compd 625:18–25
46. Norde H (1979) J Appl Phys 50:5052–5054
47. Yakuphanoglu F, Shah M, Farooq WA (2011) Acta Phys Pol A 120:558–562
48. Elgazzar E, Tataroglu A, Al-Ghamdi AA, Al-Turki Y, Farooq WA, El-Tantawy F, Yakuphanoglu F (2016) Appl Phys A 122(1-9):617
49. Mekki A, Dere A, Mensah-Darkwa K, Al-Ghamdi A, Gupta RK, Harrabi K, Farooq WA, El-Tantawy F, Yakuphanoglu F (2016) Synth Met 217:43–56
50. Kazım S, Ali V, Zulfequar M, Mazharul Haq M, Husain M (2007) Phys B 393:310–315
51. Mishra SK, Srivastava RK, Prakash SG, Yadav RS, Panday AC (2016) Opto-Electron Rev 18:467–473
52. Alyamani A, Tataroglu A, El Mir L, Al-Ghamdi AA, Dahman H, Farooq WA, Yakuphanoglu F (2016) Appl Phys A 122:297
53. Gupta RK, Yakuphanoglu F (2012) Sol Energy 86:1539–1545
54. Varghese B, Mukherjee B, Karthik KRG, Jinesh KB, Mhaisalkar SG, Tok ES, Sow CH (2012) J Appl Phys 111:104306
55. Camaioni N, Casalbore-Miceli G, Beggiato G, Cristani M, Summonte C (2000) Thin Solid Films 366:211–215
56. Yakuphanoglu F (2016) Compos Part B 92:151–159
57. Kanbur H, Altındal Ş, Tataroglu A (2005) Appl Surf Sci 252:1732–1738
58. Karatas S, Turut A (2004) Vacuum 74:45–53
59. Nicollian EH, Brews JR (1982) MOS Physics and Technology. Wiley, New York
60. Kaya A, Yucedag İ, Altındal Ş, Altunpak Y, Vural Ö (2016) journal of Materials and Electronic Devices 1:6–13
61. Hendi AA, Yakuphanoglu F (2016) J Alloys Compd 665:418–427
62. Tombak A, Ocak YS, Asubay S, Kilicoglu T, Ozkahraman F (2014) Mater Sci Semicond Process 24:187–192
63. Altındal S, Uslu H (2011) J Appl Phys 109:074503. (7 pages)
64. Tataroglu A, Al-Ghamdi AA, El-Tantawy F, Farooq WA, Yakuphanoglu F (2016) Appl Phys A 122(1-6):220